Semarak International Journal of
Fundamental and Applied Mathematics

Journal homepage:
https://semarakilmu.my/index.php/sijfam/index
ISSN: 3030-5527

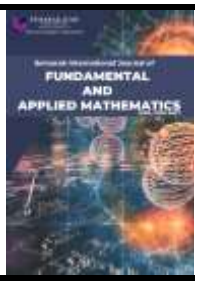

Numerical Analysis of Mixing Tank with Top Entry and Side Entry Agitator Using Computational Fluid Dynamics

Reyhan Kevin Akmal Setia Abdrian[1,*], Syifa Habli Awaliah[2], Reisya Qanita Fitriani[2]

[1] Department of Mechanical Engineering, Faculty of Engineering, Diponegoro University, Indonesia
[2] Department of Physics, Faculty of Mathematics and Natural Sciences, University of Indonesia, Indonesia

ARTICLE INFO

Article history:
Received 20 March 2025
Received in revised form 19 April 2025
Accepted 23 May 2025
Available online 30 June 2025

Keywords:
Fuel mixing process; storage tank; agitator; CFD

ABSTRACT

The procedure of mixing fuel in storage tanks is critical for ensuring fuel homogeneity and quality prior to distribution. The use of agitators as stirring devices in storage tanks helps to reduce stratification and accelerate mixing. This study used Computational Fluid Dynamics (CFD) with ANSYS 2024R2 using the $k-\varepsilon$ realizable model approach to evaluate the effectiveness of agitators at 300 and 600 rpm in optimizing the fuel mixing process for heavy naphtha and paraffin into a homogeneous product for public vehicles. Simulations were run to determine the impact of rotational speed, impeller type, and agitator position on flow distribution and mixing times. The results showed that the side entry agitator had a higher torque than the top entry agitator, reaching 3,663 Nm at 300 rpm and 14,997 Nm at 600 rpm, compared to 3,266 Nm and 13,416 Nm for the top entry agitator. Consequently, the power required for side entry agitators was 115.054 kW (300 rpm) and 942.261 kW (600 rpm), while top entry agitators required 102.585 kW (300 rpm) and 842.927 kW (600 rpm). Pressure distribution was highest in the side entry agitator at 600 rpm, leading to a stronger wall shear distribution and faster mixing. Mixing time was significantly reduced with side entry 600 rpm, achieving 75 seconds, compared to 400 seconds for top entry 600 rpm. Additionally, placing the agitator in the vertical center position produced a more equal flow pattern, accelerated homogeneity, and prevented fuel-phase separation. Once the mixing process was complete, the final fuel density was recorded at 722.1 kg/m³. These findings have significant implications for creating more reliable and energy-efficient blending systems in the energy industry.

1. Introduction

The oil and gas sector are undergoing fundamental and multidimensional upheavals, driven by a complex interplay of economic volatility, rapid technological innovation, and altering geopolitical situations. Fluctuating global demand, fluctuating energy policies, and the rapid transition to renewable alternatives are forcing industry participants to reconsider traditional strategies and adopt more adaptable, forward-thinking ways. Meanwhile, advances in digitization, automation, and artificial intelligence are transforming exploration, production, and operating efficiency, creating

* *Corresponding author.*
E-mail address: reyhankevinnn@students.undip.ac.id

https://doi.org/10.37934/sijfam.6.1.113

both possibilities and disruptions. Geopolitical concerns, supply chain vulnerabilities, and regulatory challenges all contribute to greater complexity, impacting investment decisions and transforming global energy markets. These converging dynamics are reshaping the industry's future, necessitating resilience, strategic agility, and continual innovation to navigate an increasingly uncertain and interconnected energy landscape [1]. Crude oil blending in refineries is a very complex process driven by a number of interdependent parameters and painstakingly planned actions, all with the goal of increasing operational efficiency and total profitability. To achieve desired product standards while reducing processing problems, distinct crude streams must be carefully selected and proportioned taking API gravity, sulfur concentration, viscosity, and distillation curves into account. Advanced analytical techniques and real-time monitoring systems are used to evaluate feedstock quality, forecast production outcomes, and optimize blending tactics. Market dynamics, regulatory compliance, and equipment limits all add levels of complexity, requiring a precise balance between economic objectives and technological viability. Finally, successful crude blending requires constant optimization, data-driven decision-making, and strategic foresight [2].

Crude oil is processed in numerous stages to produce a fuel that is suitable for use and meets regulations. The mixing method is a common method used in crude oil processing. This process mixes many types of hydrocarbon molecules with the goal of extracting the highest quality chemicals from crude oil, which may then be utilized as fuel [3]. In addition, the mixing process can improve cost efficiency in the fuel supply chain. Before crude oil is mixed to add hydrogen sulfide, it undergoes a series of steps that begin with the extraction of crude oil from a liquid natural gas (LNG) carrier, followed by the distribution of crude oil via a pipe to the crude oil storage tank. Once all of the crude oil is in the tank, the mixing process can begin [4,5].

In industrial mixing processes, a wide range of impeller types are carefully selected and deployed, with each design optimized to satisfy the unique requirements of individual applications. Fluid viscosity, desired flow patterns, shear sensitivity, and mixing intensity are all important considerations for establishing the best impeller arrangement. Axial flow impellers, for example, enable efficient bulk flow and homogenization, but radial flow designs produce large shear forces, making them suitable for dispersing immiscible phases or breaking down particles. Furthermore, hybrid or custom-engineered impellers may be used to navigate complicated mixed conditions while maintaining energy efficiency, process scalability, and equipment lifetime [6,7]. The careful selection and accurate calibration of impeller geometry, speed, and placement are essential for process efficiency, product uniformity, and overall operational performance [8]. The delicate interplay of blade or impeller geometry, which includes size, shape, pitch, and surface area, has a significant impact on the effectiveness and efficiency of mixing in complex industrial processes. The design and configuration of these mixing elements control fluid dynamics, turbulence intensity, and shear forces, all of which are critical for attaining uniform component distribution, optimal mass transfer, and consistent product quality. Variations in impeller diameter, blade angle, and rotational speed can significantly modify flow patterns, affecting mixing time, energy consumption, and the capacity to handle viscous or multiphase systems. As a result, choosing the right impeller design necessitates a comprehensive consideration of process requirements, material qualities, and performance objectives to ensure seamless integration and long-term operational success [9-13].

The strategic placement of impellers, whether top-entry or side-entry, has a significant impact on mixing performance, power dynamics, and overall energy efficiency in stirred tank systems. This crucial design option controls flow patterns, turbulence distribution, and shear intensity, all of which have a direct impact on mix homogeneity, heat transfer rates, and mass dispersion efficiency. Top-entry impellers often generate strong axial or radial flow, making them excellent for high-viscosity fluids or operations that require deep tank penetration, whereas side-entry impellers are commonly

used in large-volume tanks or to reduce vortex formation and silt building. The interaction of impeller orientation, rotational speed, and vessel geometry demands careful optimization to balance energy consumption with process goals, resulting in consistent product quality and long-term operating stability [14-17].

In a laboratory-scale study, a floating roof storage tank was modelled and represented using Computational Fluid Dynamics (CFD) to compare experimental and theoretical results [18]. The study found that the mixing time in the 45° jet angle setup was shorter than in the other setups. Additionally, CFD methods were used to investigate the impact of impeller position on mixing time for tank homogenization [19-21]. Research on large-scale tanks using CFD methods yields two results: in steady state conditions, increasing the number of agitators installed in the tank increases flow velocity throughout the tank, whereas in unsteady state conditions, the more agitators used accelerates the homogenization process [22]. Research on the homogenization process of crude oil in a pilot scale tank using the CFD approach with an impeller revealed that the CFD simulation findings were in good agreement with experimental data collected at two distinct places in the tank.

Previous research on the analysis of homogeneity in a stirred tank holding 70% diesel and 30% biodiesel using the CFD approach showed that homogeneity can be attained quickly depending on the rotational speed of the impeller. The faster the impeller rotates, the shorter the mixing time required to attain homogeneity [23].

Until now, there has been no research that specifically discusses the mixing of fluids between naphtha and paraffin in a fast mixing time. The current study will discuss about the storage tank filled with heavy naphtha and paraffin. The main output of this product is the mixing time of the two fluids to become homogeneous, where the product will become the main fuel for public vehicles. This storage tank has a variety of agitator placements, namely top entry and side entry agitators, with the impeller type in the form of a marine impeller because it can distribute good flow during the mixing process. The rotation speed will also be varied in this study, each in the form of 300 rpm and 600 rpm. The contour in the form of pressure and the velocity will be displayed in this study to determine the optimal results of the fluid mixing process in the storage tank.

2. Methodology

2.1 Design of the Storage Tank

This research will combine heavy naphtha and paraffin into a homogeneous product at 30 ambient temperatures in the form of gasoline which will later be used in public vehicles with the top entry and side entry agitator. Table 1 will describe the geometric dimensions of the storage tank and the impeller which will be the main parameters in this study, in addition it will also explain the main parameters in this study. Figure 1 will also provide an overview of the dimensions of the storage tank and the impeller that will be used.

Table 1
Data for Experimental of Storage Tank

Parameters	Value	Units
$\rho_{heavy\ naphtha}$	735.9	kg/m^3
$\rho_{paraffin}$	640	kg/m^3
$\mu_{heavy\ naphtha}$	0.077386	Pa.s
$\mu_{paraffin}$	0.012	Pa.s
A	2000	mm
B	4000	mm
C	1000	mm
D	400	mm
E	1000	mm
F	45	mm
G	20	mm
H	12.8	mm

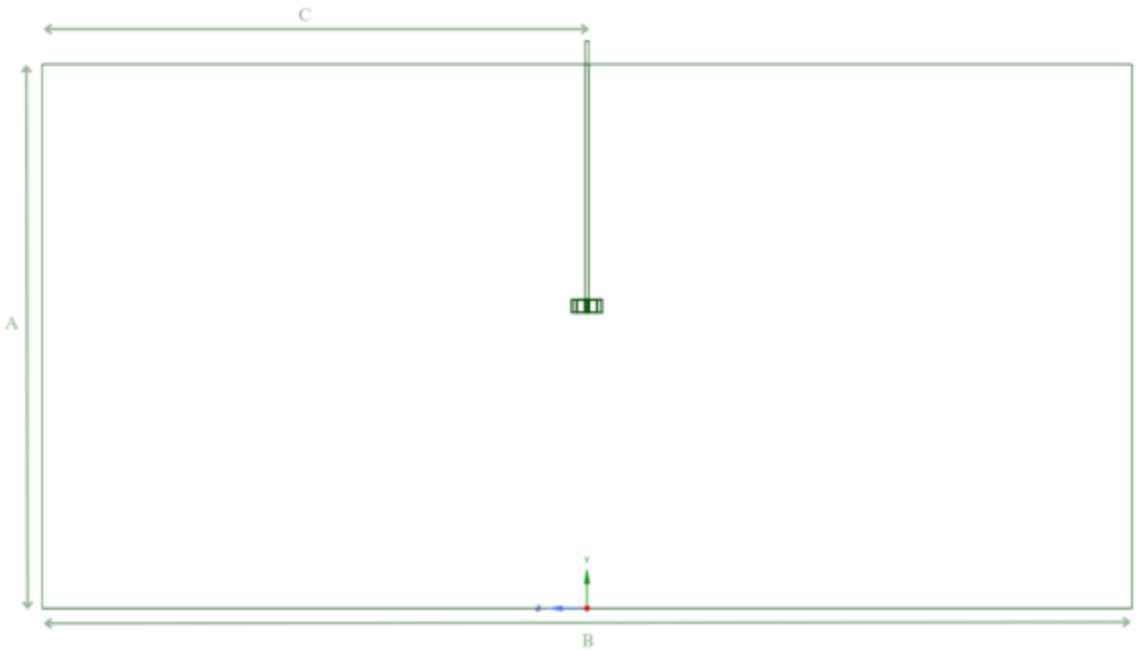

(a)

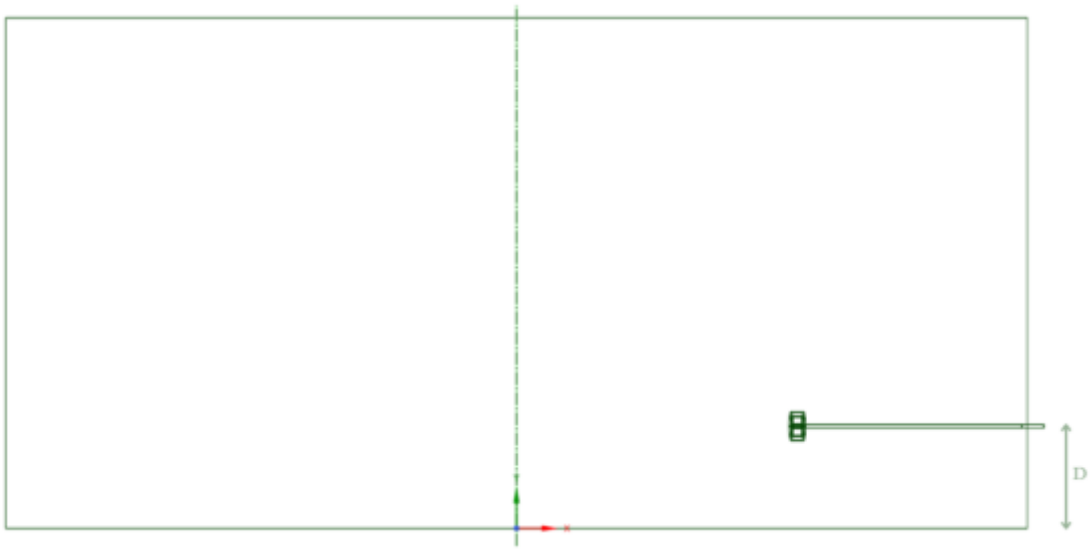

(b)

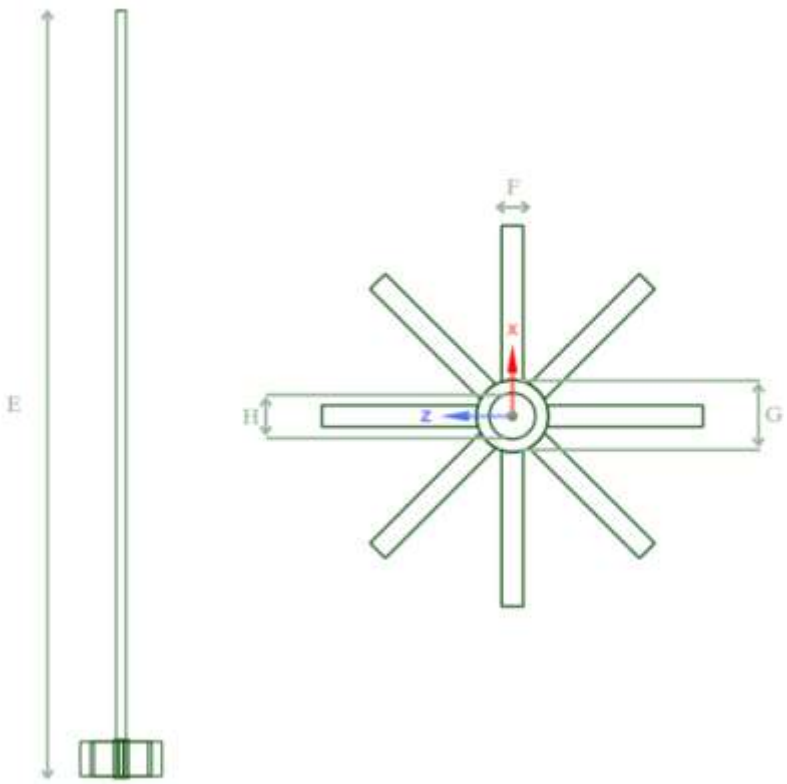

(c)

Fig. 1. Geometry dimension of (a) top-entry agitator for storage tank, (b) side-entry agitator for storage tank, and (c) impeller

2.2 Governing Equation

The fluid flow pattern in the fermenter tank was calculated in this study using the Navier-Stokes equation. Newtonian fluids with constant density and velocity were calculated using the continuity and momentum equations. The flow in the x, y, and z directions was described using the continuity equation [24,25].

Continuity:

$$\frac{\partial}{\partial x}(\rho u) + \frac{\partial}{\partial y}(\rho v) + \frac{\partial}{\partial z}(\rho w) = 0 \tag{1}$$

x-momentum:

$$\rho g_x - \frac{\partial P}{\partial x} + \mu \left(\frac{\partial^2 u}{\partial x^2} + \frac{\partial^2 u}{\partial y^2} + \frac{\partial^2 u}{\partial z^2}\right) = \rho \frac{du}{dt} \tag{2}$$

y-momentum:

$$\rho g_y - \frac{\partial P}{\partial y} + \mu \left(\frac{\partial^2 v}{\partial x^2} + \frac{\partial^2 v}{\partial y^2} + \frac{\partial^2 v}{\partial z^2}\right) = \rho \frac{dv}{dt} \tag{3}$$

z-momentum:

$$\rho g_z - \frac{\partial P}{\partial z} + \mu \left(\frac{\partial^2 w}{\partial x^2} + \frac{\partial^2 w}{\partial y^2} + \frac{\partial^2 w}{\partial z^2}\right) = \rho \frac{dw}{dt} \tag{4}$$

where t is time, P is pressure, ρ is density, μ is viscosity, and u, v, and w are the velocity components in the x,y,$and\ z$ axes.

2.3 Turbulence Models

The fluid turbulence model in the fermenter tank is computed using a realizable $k-\varepsilon$ model. An achievable $k-\varepsilon$ mathematical model considers the connection between the definition of eddy viscosity and the Boussinesq equation [26,27]. This method's advantage is its comparatively low computing cost. For shear flows with a single turbulent shear stress, the Boussinesq hypothesis for forecasting isotropic turbulent viscosity typically performs well. When applied to boundary layer properties in huge pressure gradients, segregated flows, and circulations, realizable $k-\varepsilon$ models produce improved predictions [28,29].

The Reynolds stress and mean velocity gradient are related by the Boussinesq hypothesis approach in the following way:

$$-\rho\overline{u_i'uu_j'} = \mu\left(\frac{\partial u_i}{\partial x_j}+\frac{\partial u_j}{\partial x_i}\right)-\frac{2}{3}\left(\rho k+\mu_t\ \frac{\partial u_k}{\partial x_k}\right)\delta_{ij} \tag{5}$$

μ_t as the viscosity of turbulent was defined as

$$\mu_t = \rho C_\mu\ \frac{k^2}{\varepsilon} \tag{6}$$

$k-\varepsilon$ transport equations models for Realizable is:

$$\frac{\partial}{\partial t}(\rho k)+\frac{\partial}{\partial x_j}(\rho k u_j) = \frac{\partial}{\partial x_j}\left[\left(\mu+\frac{\mu_t}{\sigma_k}\right)\ \frac{\partial k}{\partial x_j}\right]+G_k+G_b-\rho\varepsilon-Y_M+S_k \tag{7}$$

$$\frac{\partial}{\partial t}(\rho \varepsilon)+\frac{\partial}{\partial x_j}(\rho \varepsilon u_j) = \frac{\partial}{\partial x_j}\left[\left(\mu+\frac{\mu_t}{\sigma_\varepsilon}\right)\ \frac{\partial \varepsilon}{\partial x_j}\right]+\rho C_1 S\varepsilon-C_2\ \frac{\varepsilon^2}{k+\sqrt{v\varepsilon}}+C_{1\varepsilon\frac{\varepsilon}{k}}C_{3\varepsilon G_b+S_\varepsilon} \tag{8}$$

and

$$C_1 = \max\left[0.43\ \frac{\eta}{\eta+5}\right], \eta = S\ \frac{k}{\varepsilon},\ S=\sqrt{2S_{ij}S_{ij}} \tag{9}$$

The model constant value is $C_{1\varepsilon}=1.44$, $C_{2\varepsilon}=1.92$, $C_\mu=0.09$, $\sigma_k=1.0$, $\sigma_\varepsilon=1.3$. In this equation, represents the generation of turbulence kinetic energy due to mean velocity gradients, G_b represents the generation of turbulence kinetic energy due to buoyancy, The changing dilatation's contribution to compressible turbulence is represented by Y_M. Two constants are C_1 and $C_{1\varepsilon}$. The turbulent Prandtl numbers for k and ε are σ_k and σ_ε, respectively. User-defined source words are S_k and S_ε [26].

2.4 Computational Methodology

This study was solved by Ansys Fluent 2024R2 solver for solving the equation of flow in the storage tank modelling. The domain flows are utilized by 2-zone Multiple Reference Frame (MRF) with name Stationary Domain and Rotary Domain. Meanwhile, because it was thought that the fluid

did not reach the top of the tank, specific shear conditions were applied there [30]. Figure 2 show the boundary conditions set for the storage tank models. The time step in each simulation portion was established in relation to the impeller speed, which ranged from 300 to 600 rpm. As seen in Figure 3, the poly-hexcore mesh was utilized across the domain.

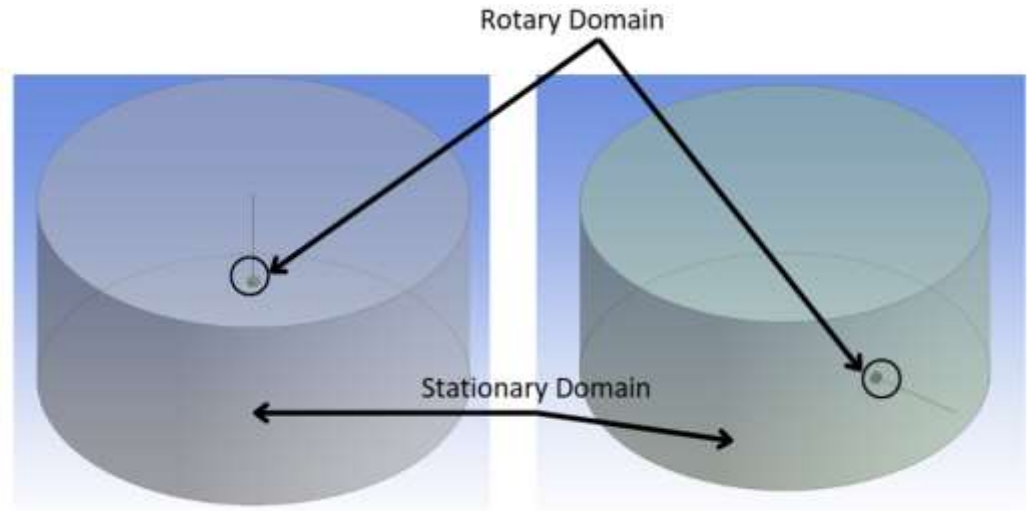

Fig. 2. Adopted boundary conditions for the CFD model

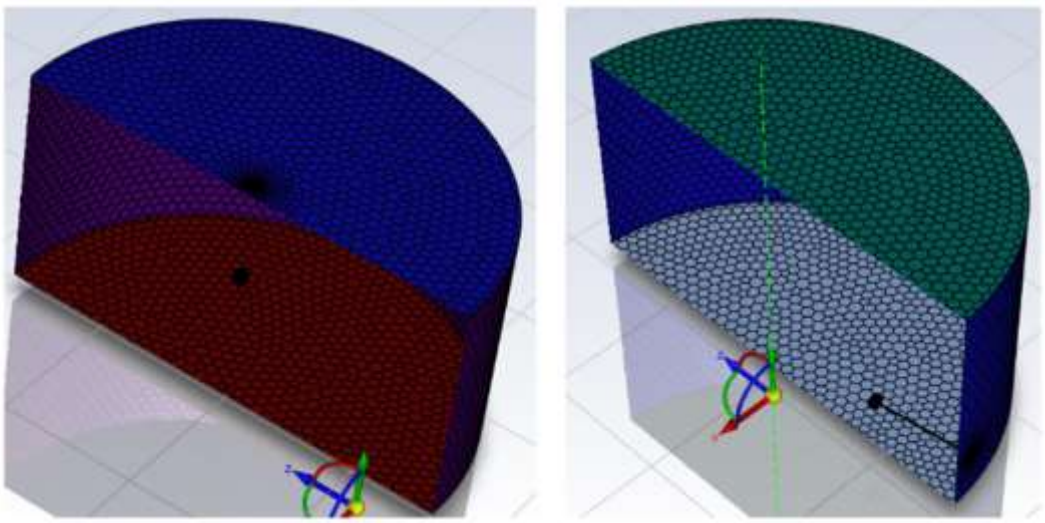

Fig. 3. Storage tank section model CFD meshing

3. Results and Discussion

3.1 Torque and Power Comparation Between Top Entry and Side Entry Agitator

Based on the analysis results of the top entry and side entry agitator tanks using rotational speeds of 300 rpm and 600 rpm, the results are as shown in Table 2, where it can be seen that the torque has different variations. This is influenced by the rotational speed and placement of the agitator. Side entry agitators often induce a radial flow, which can be less efficient compared to the axial flow typically induced by top entry agitators. Radial flow can create more turbulence and resistance, thereby increasing the torque required to maintain the same mixing efficiency [31].

Table 2
Result of the Torque

Type of Agitator Placement	Rotation Speed (rpm)	Torque (Nm)
Top Entry	300	3,266
	600	13,416
Side Entry	300	3,663
	600	14,997

As is known that 1 rpm = 0.10472 rad/s, therefore we can find out the power (in kW units) by multiplying the torque (taw) by the rotational speed that has been converted into rad/s units. It is obtained for the top entry agitator with a rotational speed of 300 rpm is 102.585 kW, and 600 rpm is 842.927 kW. Then for the side entry agitator with a rotational speed of 300 rpm has a power of 115.054 kW, and for a rotational speed of 600 rpm has a power of 942.261 kW. Figure 4 shows a comparison graph between each type of agitator placement and rotational speed.

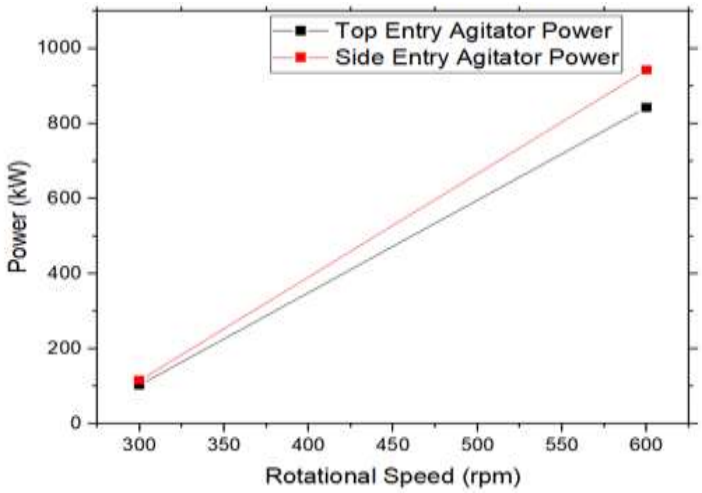

Fig. 4. Correlation between rotational speed and power

3.2 Pressure Distribution

Figure 5 shows the pressure distribution that occurs on the impeller during mixing conditions in the storage tank. It can be seen that the greatest pressure is found on the side entry agitator with a rotational speed of 600 rpm. This occurs because the fluid flow tends to enter the tank horizontally, resulting in a greater pressure difference along the distance from the impeller to the tank wall. In addition, on the side entry agitator, the friction force is higher on the tank surface, because the impeller is located on the side. This causes pressure accumulation on the sides of the tank and a greater pressure distribution compared to the top entry agitator which is directed vertically and has a more direct and more symmetrical flow.

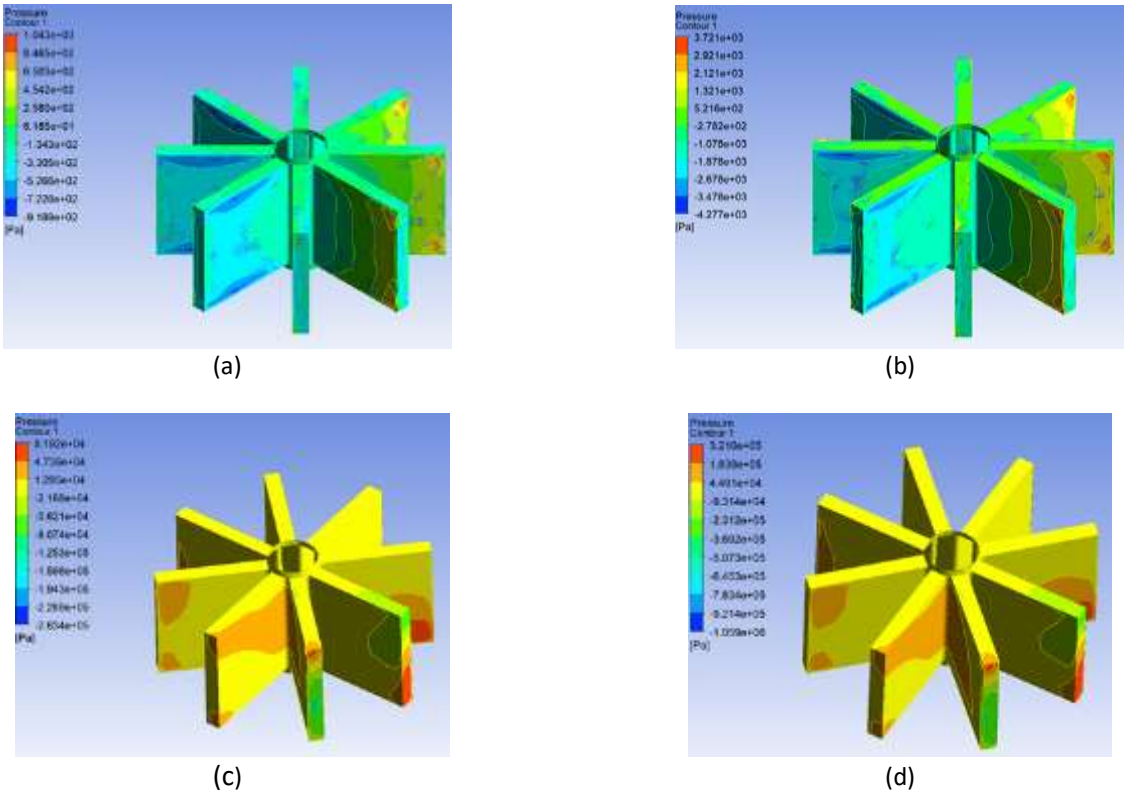

(a) (b)

(c) (d)

Fig. 5. Pressure distribution between (a) top entry agitator with 300 rpm, (b) top entry agitator with 600 rpm, (c) side entry agitator with 300 rpm, (d) side entry agitator with 600 rpm

Figure 6 will also show the graph of the relationship between the pressure on the impeller and the pressure distribution in the storage tank. It is more clearly seen that the side entry agitator with a rotational speed of 600 rpm has a much larger pressure distribution than the others.

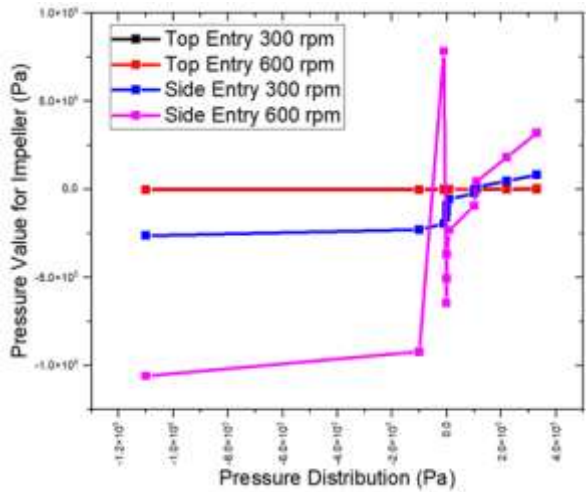

Fig. 6. Pressure distribution graphics

3.3 Wall Shear Distribution

Technically, wall shear is a shear stress that arises due to differences in fluid velocity near the surface wall. When fluid flows, the fluid layer that is very close to the wall (boundary layer) will slow

down due to friction with the wall surface [32]. Figure 7 shows the distribution of wall shear on the impeller during the mixing process.

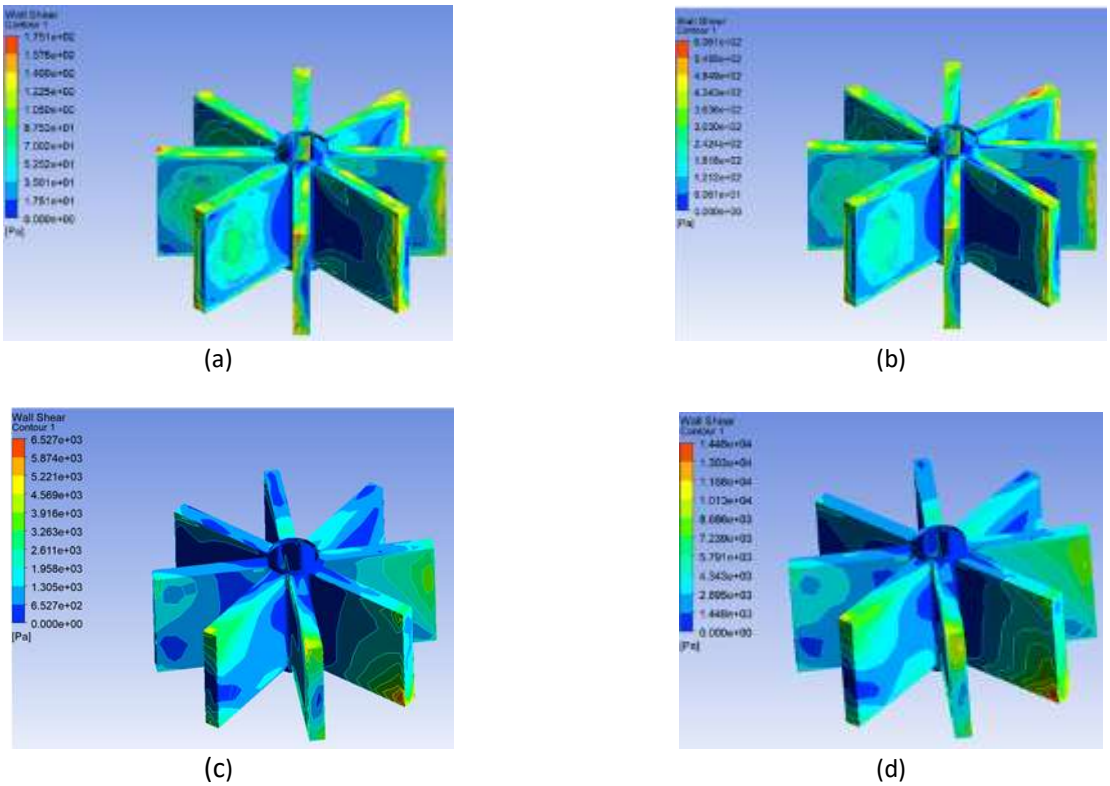

Fig. 7. Wall shear distribution between (a) top entry agitator with 300 rpm, (b) top entry agitator with 600 rpm, (c) side entry agitator with 300 rpm, (d) side entry agitator with 600 rpm

As shown in Figure 8, the largest wall shear occurs at the side entry agitator at a speed of 600 rpm. This impeller directs the fluid horizontally or diagonally, producing a greater shear force on the tank wall closer to the impeller. This flow causes a steeper velocity gradient near the wall and thus produces greater wall shear around that area.

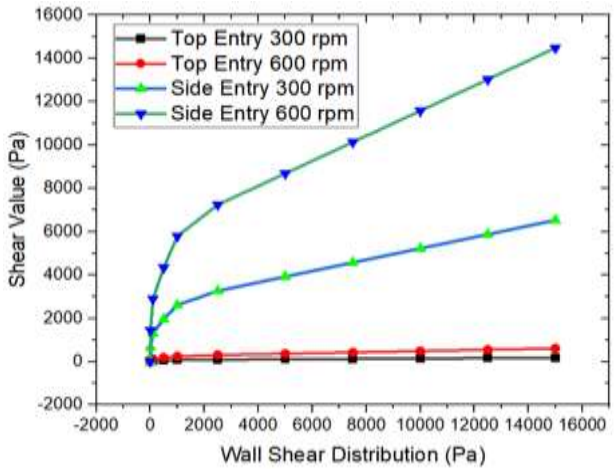

Fig. 8. Wall shear distribution graphics

3.4 Velocity Distribution

Figure 9 shows the velocity profile of the agitator working in the storage tank. It can be seen that the side entry agitator has a very different flow profile from the top entry agitator. This can happen because in the top entry agitator the velocity profile tends to be radial, spreading from the center of the impeller in all directions, while in the side entry agitator the velocity profile is more directional, forming a strong horizontal flow. It can be seen in Figure 9d because the impeller rotation speed is at 600 rpm, therefore the velocity profile is larger than the others

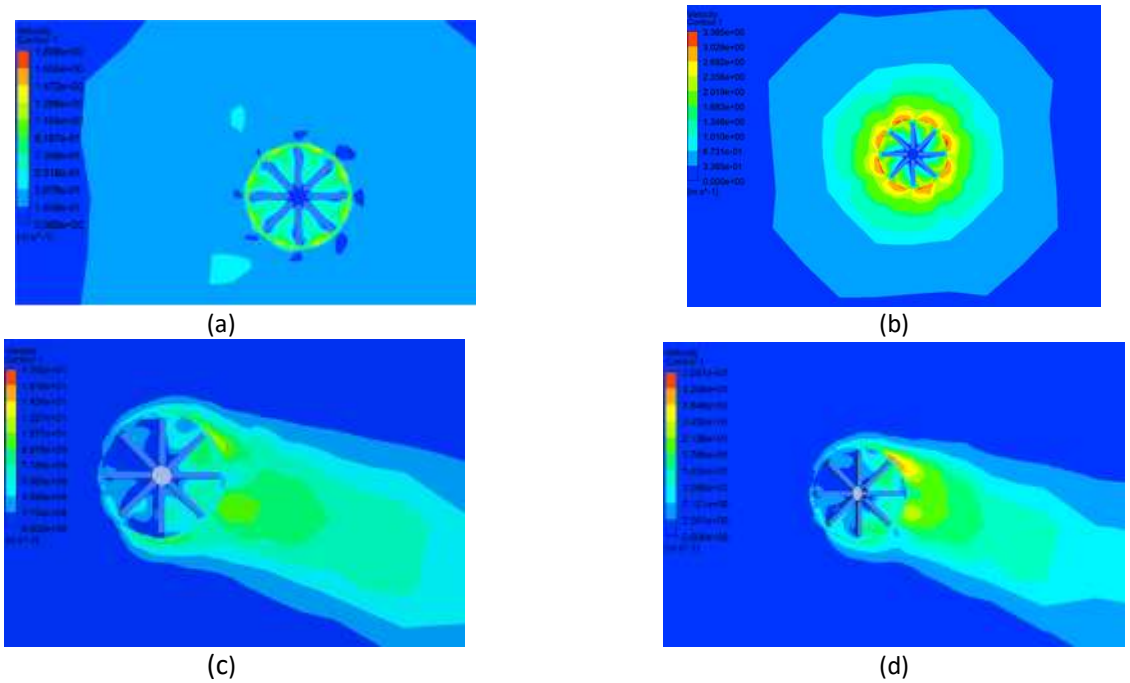

Fig. 9. Velocity distribution between (a) top entry agitator with 300 rpm, (b) top entry agitator with 600 rpm, (c) side entry agitator with 300 rpm, (d) side entry agitator with 600 rpm

3.5 Mixing Time Results

Table 3 shows the mixing time data for each agitator with side entry and top entry positions. Side entry agitators are more capable of imparting mechanical energy directly to the fluid along the tank walls, which increases turbulence and flow velocity throughout the tank. This results in faster mixing times throughout the tank volume. The density obtained in the mixing process until homogeneous is 722.1 kg/m^3.

Table 3
Result of mixing time

Type of Agitator Placement	Rotation Speed (rpm)	Time (s)
Top Entry	300	5000
	600	400
Side Entry	300	1500
	600	75

4. Conclusions

In this study, which varied the placement of the agitator at the side entry and top entry positions on the storage tank, it was found that the torque can have a greater value at the side entry placement because it has a radial flow so that it can distribute better turbulence. Then because the friction force due to turbulence at the side entry agitator is greater, therefore the pressure and wall shear are greater at the impeller with the side entry agitator position. This also affects the mixing time, where the mixing time is much faster at the side entry agitator, and a higher rotational speed will provide more efficient time in the mixing process, so that it can provide time efficiency in the mixing process.

Acknowledgement
This research was not funded by any grant.

References
[1] D'Odorico, Paolo, Kyle Frankel Davis, Lorenzo Rosa, Joel A. Carr, Davide Chiarelli, Jampel Dell'Angelo, Jessica Gephart et al. "The global food-energy-water nexus." *Reviews of geophysics* 56, no. 3 (2018): 456-531. https://doi.org/10.1029/2017RG000591

[2] Hou, Yan, NaiQi Wu, MengChu Zhou, and ZhiWu Li. "Pareto-optimization for scheduling of crude oil operations in refinery via genetic algorithm." *IEEE Transactions on Systems, Man, and Cybernetics: Systems* 47, no. 3 (2015): 517-530. https://doi.org/10.1109/TSMC.2015.2507161

[3] Li, Houqian, Horacio A. Aguirre-Villegas, Robert D. Allen, Xianglan Bai, Craig H. Benson, Gregg T. Beckham, Sabrina L. Bradshaw et al. "Expanding plastics recycling technologies: chemical aspects, technology status and challenges." *Green Chemistry* 24, no. 23 (2022): 8899-9002. https://doi.org/10.1039/D2GC02588D

[4] Guyonnet, Pierre, F. Hank Grant, and Miguel J. Bagajewicz. "Integrated model for refinery planning, oil procuring, and product distribution." *Industrial & Engineering Chemistry Research* 48, no. 1 (2009): 463-482. https://doi.org/10.1021/ie701712z

[5] Wang, Jishuai, and Gang Rong. "Robust optimization model for crude oil scheduling under uncertainty." *Industrial & Engineering Chemistry Research* 49, no. 4 (2010): 1737-1748. https://doi.org/10.1021/ie900358z

[6] Emmanuel, Michael. "Nucleation kinetics and flow-driven crystallization of lithium phosphate." PhD diss., Szegedi Tudomanyegyetem (Hungary), 2022. https://doi.org/10.14232/phd.11352

[7] Singh, Reshma, Baptiste Ravache, and Dale Sartor. *Transforming State-of-the-Art into Best Practice: A Guide for High-Performance Energy Efficient Buildings in India*. Lawrence Berkeley National Lab.(LBNL), Berkeley, CA (United States), 2018. https://doi.org/10.2172/1433127

[8] Zheng, Wanpeng, Xiaoyong Gao, Fuyu Huang, Xin Zuo, and Xiaozheng Chen. "Integrated optimization of crude oil procurement planning and blending scheduling for property stabilization." *Computers & Chemical Engineering* 186 (2024): 108716. https://doi.org/10.1016/j.compchemeng.2024.108716

[9] Appels, Lise, Jan Baeyens, Jan Degrève, and Raf Dewil. "Principles and potential of the anaerobic digestion of waste-activated sludge." *Progress in energy and combustion science* 34, no. 6 (2008): 755-781. https://doi.org/10.1016/j.pecs.2008.06.002

[10] Lou, Fangyuan, and Nicole L. Key. "On Choosing the Optimal Impeller Exit Velocity Triangles in Preliminary Design." *Journal of Turbomachinery* 144, no. 11 (2022): 111011. https://doi.org/10.1115/1.4055151

[11] Daraz, Alsadak, Fengshou Gu, and Andrew D. Ball. "Impeller wear diagnosis in centrifugal pumps under different flow rate based on acoustic signal analysis." In *Proceedings of IncoME-VI and TEPEN 2021: Performance Engineering and Maintenance Engineering*, pp. 385-401. Cham: Springer International Publishing, 2022. https://doi.org/10.1007/978-3-030-99075-6_32

[12] Yi, Weilin, and Hongliang Cheng. "Investigation on the optimal design and flow mechanism of high-pressure ratio impeller with machine learning method." *International Journal of Aerospace Engineering* 2020, no. 1 (2020): 8855314. https://doi.org/10.1155/2020/8855314

[13] Rekstin, A. F., and Yu B. Galerkin. "The primary design method development of centrifugal compressor impellers based on the analysis of the geometrical parameters." In *AIP Conference Proceedings*, vol. 2141, no. 1. AIP Publishing, 2019. https://doi.org/10.1063/1.5122102

[14] Calabrese, Richard V., T. P. K. Chang, and P. T. Dang. "Drop breakup in turbulent stirred-tank contactors. Part I: Effect of dispersed-phase viscosity." *AIChE Journal* 32, no. 4 (1986): 657-666. https://doi.org/10.1002/aic.690320416

[15] Kamla, None Youcef, Houari Ameur, Mousaab Beloudane, Zied Driss, and Abdessalam Hadjeb. "The Rheological and Energy Study of the Blade Torsion Effect in a Vessel Stirred by Two- Blade Impeller." *CFD Letters* 16, no. 11 (2024): 82–91. https://doi.org/10.37934/cfdl.16.11.8291
[16] Benmoussa, Amine, and José C. Páscoa. "A Chamfered Anchor Impeller Design for Enhanced Efficiency in Agitating Viscoplastic Fluids." *Fluids* 9, no. 12 (2024): 288. https://doi.org/10.3390/fluids9120288
[17] Ameur, Houari. "Effect of the shaft eccentricity and rotational direction on the mixing characteristics in cylindrical tank reactors." *Chinese Journal of Chemical Engineering* 24, no. 12 (2016): 1647-1654. https://doi.org/10.1016/j.cjche.2016.05.011
[18] Vijayan, Dhanasingh Sivalinga, Eugeniusz Koda, Arvindan Sivasuriyan, Jan Winkler, Parthiban Devarajan, Ramamoorthy Sanjay Kumar, Aleksandra Jakimiuk, Piotr Osinski, Anna Podlasek, and Magdalena Daria Vaverková. "Advancements in solar panel technology in civil engineering for revolutionizing renewable energy solutions—a review." *Energies* 16, no. 18 (2023): 6579. https://doi.org/10.3390/en16186579
[19] Rahimi, Masoud. "The effect of impellers layout on mixing time in a large-scale crude oil storage tank." *Journal of Petroleum Science and Engineering* 46, no. 3 (2005): 161-170. https://doi.org/10.1016/j.petrol.2004.12.002
[20] Rahimi, Masoud, and Arsalan Parvareh. "Experimental and CFD investigation on mixing by a jet in a semi-industrial stirred tank." *Chemical Engineering Journal* 115, no. 1-2 (2005): 85-92. https://doi.org/10.1016/j.cej.2005.09.021
[21] Adepu, Janakiramulu, Rahul C. Patil, Ajay Gupta, Asit Kumar Das, Pravin Potdar, Jisna Raghavan, and Kannan Srinivasan. "Mixing in Large Crude Tanks." *Digital Refining* (2015):1–4.
[22] Karuana, Feri, Hafizh Ghazidin, Andrias R. Wimada, Muhammad P. Helios, Himawan Sutriyanto, and Maharani D. Solikhah. "Homogeneity analysis of B30 mixing results with additives in mixing tanks using computational fluid dynamics (CFD)." *Materials Today: Proceedings* 87 (2023): 141-146. https://doi.org/10.1016/j.matpr.2023.02.388
[23] Walas, Stanley M. "Chemical process equipment: selection and design." *(No Title)* (1988).
[24] Patil, Harshal, Ajey Kumar Patel, Harish J. Pant, and A. Venu Vinod. "CFD simulation model for mixing tank using multiple reference frame (MRF) impeller rotation." *ISH Journal of Hydraulic Engineering* 27, no. 2 (2021): 200-209. https://doi.org/10.1080/09715010.2018.1535921
[25] Purwanto, Sigit, Bayu Novariawan, Palupi Tri Widiyanti Suparman, Isnaini Pratiwiningrum, and Fitri Nur Kayati. "CFD Analysis and Development of Mixing Tank Design for the Fermented Starch Production Process." https://doi.org/10.37934/cfdl.16.1.95106
[26] Fluent, A. N. S. Y. S. "ANSYS Fluent Theory Guide, Release 18.0. Ansys." *Inc.: Canonsburg, PA, USA* (2017).
[27] Shekhar, S. Murthy, and S. Jayanti. "CFD study of power and mixing time for paddle mixing in unbaffled vessels." *Chemical Engineering Research and Design* 80, no. 5 (2002): 482-498. https://doi.org/10.1205/026387602320224067
[28] Shaheed, Rawaa, Abdolmajid Mohammadian, and Hossein Kheirkhah Gildeh. "A comparison of standard k–ε and realizable k–ε turbulence models in curved and confluent channels." *Environmental Fluid Mechanics* 19 (2019): 543-568. https://doi.org/10.1007/s10652-018-9637-1
[29] Phumnok, Ekaroek, Waritnan Wanchan, Matinee Chuenjai, Panut Bumphenkiattikul, Sunun Limtrakul, Sukrittira Rattanawilai, and Parinya Khongprom. "Study of hydrodynamics and upscaling of immiscible fluid stirred tank using computational fluid dynamics simulation." *CFD Lett.* 14 (2022): 115-133. https://doi.org/10.37934/cfdl.14.6.115133
[30] Baba, Ahmad Faiq, Nor Afzanizam Samiran, Razlin Abd Rashid, Izuan Amin Ishak, Zuliazura Mohd Salleh, Rais Hanizam Madon, and Muhammad Suhail Sahul Hamid. "Effect of impeller's blade number on the performance of mixing flow in stirred tank using CFD simulation method." *CFD Letters* 14, no. 5 (2022): 33-42. https://doi.org/10.37934/cfdl.14.5.3342
[31] Kim, Youn-Jea, and Jung-Hoon Hwang. "A numerical analysis on the flow characteristics in a helical screw agitator with a draught tube." In *Fluids Engineering Division Summer Meeting*, vol. 47500, pp. 1493-1500. 2006.
[32] Haritonidis, Joseph H. "The measurement of wall shear stress." In *Advances in fluid mechanics measurements*, pp. 229-261. Berlin, Heidelberg: Springer Berlin Heidelberg, 1989. https://doi.org/10.1007/978-3-642-83787-6_6